On the Implementation and Further Validation of a Time Domain Boundary Element Method Broadband Impedance Boundary Condition

*Fang Q. Hu**
Old Dominion University, Norfolk, VA 23529, USA

Douglas M. Nark†
NASA Langley Research Center, Hampton, VA 23681-2199, U.S.A

A time domain boundary integral equation with Burton-Miller reformulation is presented for acoustic scattering by surfaces with liners in a uniform mean flow. The Ingard-Myers impedance boundary condition is implemented using a broadband multipole impedance model and converted into time domain differential equations to augment the boundary integral equation. The coupled integral-differential equations are solved numerically by a March-On-in-Time (MOT) scheme. While the Ingard-Myers condition is known to support Kelvin-Helmholtz instability due to its use of a vortex sheet interface between the flow and the liner surface, it is found that by neglecting a second derivative term in the current time domain impedance boundary condition formulation, the instability can be effectively suppressed in computation. Proposed formulation and implementation are validated using NASA Langley Research Center Grazing Flow Impedance Tube (GFIT) experimental dataset with satisfactory results. Moreover, a minimization procedure for finding the poles and coefficients of the broadband multiple impedance model is formulated in this paper by which, unlike the commonly used vector-fitting method, passivity of the model is ensured. Numerical tests show the proposed minimization approach is effective for modeling liners that are commonly used in aeroacoustics applications.

I. Introduction

Acoustical liners are an effective tool for sound absorption. It is important for computational tools of sound scattering prediction to include treated surfaces. Acoustical properties of a liner are characterized by the impedance boundary condition in the frequency domain. Previously, coupling of an impedance boundary condition with a Time Domain Boundary Element Method (TDBEM) has been studied numerically under the assumption of no mean flow.[19] In this paper, implementation of a broadband impedance boundary condition with a nonzero mean flow is considered. In particular, the Time Domain Boundary Integral Equation (TDBIE) with Burton-Miller reformulation[3] is presented with both the acoustic pressure and its surface normal derivative terms retained for the purpose of implementing the impedance boundary condition.

In the presence of a nonzero uniform mean flow, the impedance condition is commonly implemented by the Ingard-Myers formulation.[12,16] In this work, the Ingard-Myers formulation is applied and coupled with TDBIE. The liner impedance as a function of frequency are first modeled by a broadband multipole expansion and then converted into time domain differential equations that relate the pressure and its normal derivative on the liner surface. It is well-known that the Ingard-Myers condition can support Kelvin-Helmholtz instability waves due to its use of a vortex sheet interface between the flow and the liner surface.[20] In this study, it is found that by neglecting a second derivative term in the current time domain impedance boundary condition formulation, the Kelvin-Helmholtz instability can be effectively suppressed in computation.

*Professor, Department of Mathematics and Statistics, AIAA Associate Fellow
†Senior Research Scientist, Structural Acoustics Branch, Research Directorate, AIAA Associate Fellow

To implement the impedance condition in the time domain, the liner impedance as a function of frequency is approximated by a broadband multipole expansion that matches the experimentally measured/educed impedance. In the literature, the multipole model is often computed using the vector-fitting method.[9] The vector-fitting method converts a nonlinear optimization problem to a series of linear least square problems. However, a drawback of the vector-fitting method is that the passivity condition is not ensured and needs to be separately checked or enforced.[10] In this paper, we describe a minimization method for finding the poles and coefficients of the multipole model in which the passivity is always satisfied.

To validate the formulation and numerical implementation, an experimental dataset from the NASA Langley Research Grazing Flow Impedance Tube (GFIT) is used for comparison with computational results.[13] The inherently internal duct propagation problem is cast as an external scattering problem in an open-ended duct configuration. The source term for the time domain boundary integral equation is formulated such that an incident plane wave mode is generated inside the duct. The time domain solution of the plane wave scattered by a section of liner installed inside the duct is converted to frequency domain solutions and compared with the GFIT experimental measurements.

The rest of the paper is organized as follows. Detailed derivation of TDBIE with Burton-Miller reformulation and the time domain impedance boundary condition with a uniform mean flow is given in Sec. II. A technique of finding the poles and coefficients of the broadband impedance multipole model is discussed in Sec. III. Sec. IV gives the details on the discretization for TDBIE coupled with the impedance boundary condition. Sec. V presents a numerical example of the formulation and discretization discussed in the present paper as well as comparisons between the computational and experimental results. Sec. VI has the concluding remarks.

II. Mathematical formulation

II.A. Time domain boundary integral equation with lined surface in flow

Under the assumption of a constant mean flow $\boldsymbol{U}$, propagation and scattering of acoustic pressure $\boldsymbol{p}(\boldsymbol{r},t)$ is governed by the convective wave equation:

$$\left(\frac{\partial}{\partial t}+\boldsymbol{U}\cdot\nabla\right)^2 p - c^2\nabla^2 p = s(\boldsymbol{r},t), \tag{1}$$

where $\boldsymbol{r}=(x,y,z)$ is the position vector, t is time, c is the speed of sound, and $s(\boldsymbol{r},t)$ represents a prescribed acoustic source term. Here, $\nabla=(\partial/\partial x,\partial/\partial y,\partial/\partial z)$. The convective wave equation (1), together with the homogeneous initial conditions,

$$p(\boldsymbol{r},t)=\frac{\partial p}{\partial t}(\boldsymbol{r},t)=0 \ \text{ as } \ t\to-\infty, \tag{2}$$

can be converted into an integral relation as follows:[11]

$$4\pi p(\boldsymbol{r}',t') = \frac{1}{c^2}\int_{V_s}\frac{1}{\bar{R}}s(\boldsymbol{r},t'_R)d\boldsymbol{r} + \int_S\left[G_0\frac{\partial p}{\partial\tilde{n}}(\boldsymbol{r}_s,t'_R) - \frac{\partial G_0}{\partial\bar{n}}\left(p(\boldsymbol{r}_s,t'_R)+\frac{\bar{R}}{c\alpha^2}\frac{\partial p}{\partial t}(\boldsymbol{r}_s,t'_R)\right)\right]d\boldsymbol{r}_s \tag{3}$$

in which V_s denotes the region where the source term is non-zero, S denotes the scattering surface, and $\boldsymbol{r}'$ is an off-surface field point and t' is the observer time. Also in the above,

$$G_0=\frac{1}{\bar{R}(\boldsymbol{r}_s,\boldsymbol{r}')},\quad \bar{R}(\boldsymbol{r},\boldsymbol{r}')=\sqrt{\left[\boldsymbol{M}\cdot(\boldsymbol{r}-\boldsymbol{r}')\right]^2+\alpha^2|\boldsymbol{r}-\boldsymbol{r}'|^2},\qquad t'_R=t'+\boldsymbol{\beta}\cdot(\boldsymbol{r}'-\boldsymbol{r}_s)-\frac{\bar{R}}{c\alpha^2} \tag{4}$$

in which

$$\boldsymbol{M}=\frac{\boldsymbol{U}}{c},\ \ \alpha=\sqrt{1-|\boldsymbol{M}|^2},\ \ \boldsymbol{\beta}=\frac{\boldsymbol{U}}{c^2-|\boldsymbol{U}|^2}=\frac{\boldsymbol{U}}{c^2\alpha^2}=\frac{\boldsymbol{M}}{c\alpha^2}. \tag{5}$$

The *modified normal derivative* and the *combined normal derivative* on surface S, denoted respectively by $\partial/\partial\bar{n}$ and $\partial/\partial\tilde{n}$, appearing in (3) are defined as follows:

$$\frac{\partial}{\partial\bar{n}} = \frac{\partial}{\partial n} - M_n \cdot (\boldsymbol{M}\cdot\nabla), \quad M_n = \boldsymbol{n}\cdot\boldsymbol{M} = \boldsymbol{n}\cdot\boldsymbol{U}/c \tag{6}$$

$$\frac{\partial}{\partial\tilde{n}} = \frac{\partial}{\partial n} - \frac{M_n}{c}\left(\frac{\partial}{\partial t} + \boldsymbol{U}\cdot\nabla\right) = \frac{\partial}{\partial\bar{n}} - \frac{M_n}{c}\frac{\partial}{\partial t}. \tag{7}$$

Here, the surface normal vector $\boldsymbol{n}$ is assumed to be in the direction out of the propagation medium and into the scattering body. A boundary integral equation is formed by the limit $\boldsymbol{r}' \to \boldsymbol{r}'_s$ in (3) where $\boldsymbol{r}'_s$ denotes a boundary point on S. When $\boldsymbol{r}'_s$ is a smooth point on the scattering surface (such as any interior point on a surface element), as detailed in [11], the boundary integral equation can be written as follows:

$$2\pi p(\boldsymbol{r}'_s,t') - \int_S \left[G_0\frac{\partial p}{\partial\tilde{n}}(\boldsymbol{r}_s,t'_R) - \frac{\partial G_0}{\partial\bar{n}}\left(p(\boldsymbol{r}_s,t'_R) + \frac{\bar{R}}{c\alpha^2}\frac{\partial p}{\partial t}(\boldsymbol{r}_s,t'_R)\right)\right] d\boldsymbol{r}_s = Q(\boldsymbol{r}'_s,t') \tag{8}$$

where

$$Q(\boldsymbol{r}'_s,t') = \frac{1}{c^2}\int_{V_s}\frac{1}{\bar{R}}s(\boldsymbol{r},t'_R)d\boldsymbol{r} \tag{9}$$

For convenience of discussion, we will use p_n to denote $\partial p/\partial\tilde{n}$ in our discussions, i.e.,

$$p_n \equiv \frac{\partial p}{\partial\tilde{n}} \tag{10}$$

Eq. (3) shows that when both p and p_n are known on the scattering surface S, the solution at any field point $\boldsymbol{r}'$ can be computed directly by evaluating the integrals on its right hand side. When the scattering surface S is rigid, we have $p_n = 0$, and p can be found by solving the boundary integral equation (8) as in [11]. When surface S includes acoustic liners, p and p_n are related by an impedance condition, and by eliminating p_n through the impedance condition, the surface pressure p can again be found by the boundary integral equation (8). A numerical method for the time domain integral equation (8) when coupled with an impedance boundary condition has been recently studied in [19] for the case of no flow. The primary focus of the current paper is to study the case when the mean flow is present.

While direct numerical solution of (8) is known to be prone to long time instabilities, recent studies have shown that a Burton-Miller reformulation is effective in eliminating the instability.[5,7,11] Time domain Burton-Miller reformulation involves applying the following operator to (3) and evaluating it at surface points $\boldsymbol{r}'_s$:

$$a\frac{\partial}{\partial t'} + bc\frac{\partial}{\partial\tilde{n}'}$$

where a and b are two constants such that $a/b < 0$ (Typically, $a = -b = 1$). This leads to

$$a\left[4\pi\frac{\partial p}{\partial t}(\boldsymbol{r}',t') - \int_S G_0(\boldsymbol{r}_s,\boldsymbol{r}')\frac{\partial p_n}{\partial t}(\boldsymbol{r}_s,t'_R)d\boldsymbol{r}_s + \int_S \frac{\partial G_0}{\partial\bar{n}}(\boldsymbol{r}_s,\boldsymbol{r}')\left(\frac{\partial p}{\partial t}(\boldsymbol{r}_s,t'_R) + \frac{\bar{R}}{c\alpha^2}\frac{\partial^2 p}{\partial t^2}(\boldsymbol{r}_s,t'_R)\right)d\boldsymbol{r}_s\right]_{\boldsymbol{r}'\to\boldsymbol{r}'_s}$$

$$+bc\left[4\pi p_n(\boldsymbol{r}',t') - \frac{\partial}{\partial\tilde{n}'}\int_S G_0(\boldsymbol{r}_s,\boldsymbol{r}')p_n(\boldsymbol{r}_s,t'_R)d\boldsymbol{r}_s + \frac{\partial}{\partial\tilde{n}'}\int_S \frac{\partial G_0}{\partial\bar{n}}(\boldsymbol{r}_s,\boldsymbol{r}')\left(p(\boldsymbol{r}_s,t'_R) + \frac{\bar{R}}{c\alpha^2}\frac{\partial p}{\partial t}(\boldsymbol{r}_s,t'_R)\right)d\boldsymbol{r}_s\right]_{\boldsymbol{r}'\to\boldsymbol{r}'_s}$$

$$= a\frac{\partial Q}{\partial t'}(\boldsymbol{r}'_s,t') + bc\frac{\partial Q}{\partial\tilde{n}'}(\boldsymbol{r}'_s,t') \tag{11}$$

The limit for the first term in bracket on the left hand of side of (11) can be simplified as in [11]. To simplify the limit for the singular integrals in the second term in bracket in (11), note that we have

$$\frac{\partial}{\partial \tilde{n}'}\int_S G_0(\boldsymbol{r}_s,\boldsymbol{r'})p_n(\boldsymbol{r}_s,t'_R)d\boldsymbol{r}_s=\int_S \frac{\partial G_0}{\partial \bar{n}'}(\boldsymbol{r}_s,\boldsymbol{r'})p_n(\boldsymbol{r}_s,t'_R)d\boldsymbol{r}_s+\int_S G_0(\boldsymbol{r}_s,\boldsymbol{r'})\frac{\partial p_n}{\partial t}(\boldsymbol{r}_s,t'_R)\frac{\partial t'_R}{\partial \tilde{n}'}d\boldsymbol{r}_s \tag{12}$$

where we have

$$\frac{\partial t'_R}{\partial \tilde{n}'}=-\frac{1}{c\alpha^2}\frac{\partial \bar{R}}{\partial \bar{n}'},\quad \frac{\partial \bar{R}}{\partial \bar{n}'}=-\bar{R}^2\frac{\partial G_0}{\partial \bar{n}'},\quad G_0\frac{\partial \bar{R}}{\partial \bar{n}'}=-\bar{R}\frac{\partial G_0}{\partial \bar{n}'}$$

Furthermore, the limit of $\boldsymbol{r}\to\boldsymbol{r}'_s$ for the weakly singular integral involving p_n in (12) (the first term on the right hand side) can be found as follows:

$$\lim_{\boldsymbol{r'}\to\boldsymbol{r}'_s}\int_S \frac{\partial G_0}{\partial \bar{n}'}(\boldsymbol{r}_s,\boldsymbol{r'})p_n(\boldsymbol{r}_s,t'_R)d\boldsymbol{r}_s$$

$$=\lim_{\boldsymbol{r'}\to\boldsymbol{r}'_s}\int_S \frac{\partial G_0}{\partial \bar{n}'}(\boldsymbol{r}_s,\boldsymbol{r'})\left\{p_n(\boldsymbol{r}_s,t'_R)-p_n(\boldsymbol{r}'_s,t')\right\}d\boldsymbol{r}_s+p_n(\boldsymbol{r}'_s,t')\lim_{\boldsymbol{r'}\to\boldsymbol{r}'_s}\int_S \frac{\partial G_0}{\partial \bar{n}'}(\boldsymbol{r}_s,\boldsymbol{r'})d\boldsymbol{r}_s$$

$$=\int_S \frac{\partial G_0}{\partial \bar{n}'}(\boldsymbol{r}_s,\boldsymbol{r}'_s)p_n(\boldsymbol{r}_s,t'_R)d\boldsymbol{r}_s+2\pi p_n(\boldsymbol{r}'_s,t')$$

where we have used the following results:

$$\frac{1}{4\pi}\int_S \frac{\partial G_0}{\partial \bar{n}'}(\boldsymbol{r}_s,\boldsymbol{r'})d\boldsymbol{r}_s=\begin{cases}0 & \boldsymbol{r'}\in V,\ \text{exterior of } S\\ -\frac{1}{2} & \boldsymbol{r'}=\boldsymbol{r}'_s\in S\\ -1 & \boldsymbol{r}\in V^-,\ \text{interior of } S\end{cases} \tag{13}$$

Finally, we get the following Burton-Miller reformulation of the time domain boundary integral equation (8):

$$a\left[2\pi\frac{\partial p}{\partial t}(\boldsymbol{r}'_s,t')-\int_S G_0(\boldsymbol{r}_s,\boldsymbol{r'}_s)\frac{\partial p_n}{\partial t}(\boldsymbol{r}_s,t'_R)d\boldsymbol{r}_s+\int_S \frac{\partial G_0}{\partial \bar{n}}(\boldsymbol{r}_s,\boldsymbol{r}'_s)\left(\frac{\partial p}{\partial t}(\boldsymbol{r}_s,t'_R)+\frac{\bar{R}}{c\alpha^2}\frac{\partial^2 p}{\partial t^2}(\boldsymbol{r}_s,t'_R)\right)d\boldsymbol{r}_s\right]$$

$$+bc\left[2\pi p_n(\boldsymbol{r}'_s,t')-\int_S \frac{\partial G_0}{\partial \bar{n}'}(\boldsymbol{r}_s,\boldsymbol{r}'_s)\left(p_n(\boldsymbol{r}_s,t'_R)+\frac{\bar{R}}{c\alpha^2}\frac{\partial p_n}{\partial t}(\boldsymbol{r}_s,t'_R)\right)d\boldsymbol{r}_s\right]$$

$$-\frac{b}{c\alpha^4}\int_S \bar{R}^3\frac{\partial G_0}{\partial \bar{n}'}\frac{\partial G_0}{\partial \bar{n}}\frac{\partial^2 p}{\partial t^2}(\boldsymbol{r}_s,t'_R)d\boldsymbol{r}_s+bc\left[\int_S \frac{\partial^2 G_0}{\partial \bar{n}'\partial \bar{n}}\left(p(\boldsymbol{r}_s,t'_R)-p(\boldsymbol{r}'_s,t')+\frac{\bar{R}}{c\alpha^2}\frac{\partial p}{\partial t}(\boldsymbol{r}_s,t'_R)\right)d\boldsymbol{r}_s\right]$$

$$=a\frac{\partial Q}{\partial t'}(\boldsymbol{r}'_s,t')+bc\frac{\partial Q}{\partial \tilde{n}'}(\boldsymbol{r}'_s,t') \tag{14}$$

where all the integrals in (11) involving p have been simplified in the same way as in [11] (without the liners). On rigid surfaces, the Zero Energy Flux (ZEF) boundary condition is applied,[11] which leads to

$$p_n=\frac{\partial p}{\partial \tilde{n}}=0.$$

On treated surfaces, p and p_n are coupled through the impedance condition as described below.

II.B. Liner impedance boundary condition with flow

In this work, we assume that the mean flow is tangent or nearly tangent to the surface of liner (i.e., we assume $M_n=0$ on liner surfaces). This is expected to be the most common practical situation when liners are utilized. Consequently, the modified and combined normal derivatives as defined in Eqs. (6)-(7) will be the same as the usual normal derivative (i.e., we have $\partial p/\partial\tilde{n}=\partial p/\partial\bar{n}=\partial p/\partial n$ on liner surfaces).

In the Ingard-Myers liner impedance model, an infinitely thin vortex sheet of infinitesimally small oscillation is assumed between the mean flow and the liner surface,[12,16] as illustrated in Fig. 1. Let the displacement of the vortex sheet in the direction of the normal vector $\boldsymbol{n}$ of the liner surface be denoted as

$$\zeta = \zeta(\boldsymbol{r}, t). \tag{15}$$

Then, the displacement velocity on the surface of the liner, in the direction of its normal vector $\boldsymbol{n}$, denoted by u_w, is

$$u_w = \frac{\partial \zeta}{\partial t} \tag{16}$$

On the other hand, upon applying a linearization procedure, the displacement velocity along the vortex sheet, denoted by $u_n = \boldsymbol{u} \cdot \boldsymbol{n}$ where $\boldsymbol{u}$ is the acoustic velocity, on the side of the fluid which is moving with a mean velocity $\boldsymbol{U}$ is

$$u_n = \frac{\partial \zeta}{\partial t} + \boldsymbol{U} \cdot \nabla \zeta. \tag{17}$$

Eliminating ζ, we get the relation between u_n and u_w as follows:

$$\frac{\partial u_n}{\partial t} = \frac{\partial u_w}{\partial t} + \boldsymbol{U} \cdot \nabla u_w. \tag{18}$$

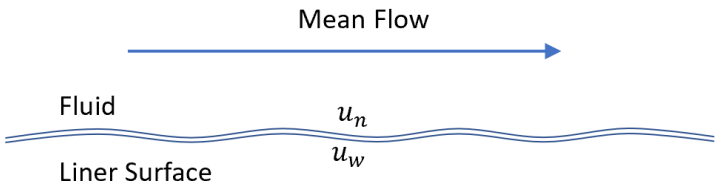

Figure 1. Illustration of Ingard-Myers liner vortex sheet model. u_n and u_w are vertical velocities of the medium and liner surface, respectively.

Now the impedance on the surface of liner is defined such that

$$\frac{\hat{p}(\boldsymbol{r}, \omega)}{\hat{u}_w(\boldsymbol{r}, \omega)} = Z(\omega), \tag{19}$$

where $Z(\omega)$ is the liner surface impedance and ω is the frequency. Here, a caret denotes the frequency domain variables. In this work, a broadband multipole expansion of the following form is used for modeling the impedance $Z(\omega)$ as a function of frequency ω:

$$Z(\omega) = (-i\omega)h_0 + R_0 + \sum_{m=1}^{M} \frac{A_m}{\lambda_m - i\omega} + \frac{1}{2} \sum_{\ell=1}^{L} \left[\frac{B_\ell + iC_\ell}{\alpha_\ell + i\beta_\ell - i\omega} + \frac{B_\ell - iC_\ell}{\alpha_\ell - i\beta_\ell - i\omega} \right] \tag{20}$$

where M and L represent, respectively, the number of single and paired poles used in the model. Multipole expansion models like (20) have been used in many recent studies on implementing the time domain impedance boundary condition.[6,14,15,17,20] The parameters in Eq. (20) are found by matching $Z(\omega)$ with given impedance values of the physical liner. Further details will be discussed in Sec. III.

Converting into time domain and assuming $e^{-i\omega t}$ sign convention, impedance condition Eq. (19) leads to

$$p(\boldsymbol{r}, t) = h_0 \frac{\partial u_w}{\partial t} + R_0 u_w(\boldsymbol{r}, t) + \sum_{m=1}^{M} A_m p_m^{(0)}(\boldsymbol{r}, t) + \sum_{\ell=1}^{L} \left[B_\ell p_\ell^{(1)}(\boldsymbol{r}, t) + C_\ell p_\ell^{(2)}(\boldsymbol{r}, t) \right] \tag{21}$$

in which

$$\frac{dp_m^{(0)}}{dt} + \lambda_m p_m^{(0)}(\boldsymbol{r},t) = u_w(\boldsymbol{r},t), \quad m = 1, ..., M \tag{22}$$

$$\frac{dp_\ell^{(1)}}{dt} + \alpha_\ell p_\ell^{(1)}(\boldsymbol{r},t) + \beta_\ell p_\ell^{(2)}(\boldsymbol{r},t) = u_w(\boldsymbol{r},t), \quad \frac{dp_\ell^{(2)}}{dt} + \alpha_\ell p_\ell^{(2)}(\boldsymbol{r},t) - \beta_\ell p_\ell^{(1)}(\boldsymbol{r},t) = 0, \quad \ell = 1, ..., L \tag{23}$$

where $p_m^{(0)}(\boldsymbol{r},t)$, $p_\ell^{(1)}(\boldsymbol{r},t)$ and $p_\ell^{(2)}(\boldsymbol{r},t)$ are auxiliary variables that are often used to facilitate computation.[6] Next, by applying the material derivative operator $\frac{\partial}{\partial t} + \boldsymbol{U}\cdot\nabla$ to Eqs. (21)-(23), and using (18), we get

$$\frac{\partial p}{\partial t} + \boldsymbol{U}\cdot\nabla p(\boldsymbol{r},t) = h_0\frac{\partial^2 u_n}{\partial t^2} + R_0\frac{\partial u_n}{\partial t} + \sum_{m=1}^{M} A_m p_m^{(0)}(\boldsymbol{r},t) + \sum_{\ell=1}^{L}\left[B_\ell p_\ell^{(1)}(\boldsymbol{r},t) + C_\ell p_\ell^{(2)}(\boldsymbol{r},t)\right] \tag{24}$$

$$\frac{dp_m^{(0)}}{dt} + \lambda_m p_m^{(0)}(\boldsymbol{r},t) = \frac{\partial u_n}{\partial t}, \quad m = 1, ..., M \tag{25}$$

$$\frac{dp_\ell^{(1)}}{dt} + \alpha_\ell p_\ell^{(1)}(\boldsymbol{r},t) + \beta_\ell p_\ell^{(2)}(\boldsymbol{r},t) = \frac{\partial u_n}{\partial t}, \quad \frac{dp_\ell^{(2)}}{dt} + \alpha_\ell p_\ell^{(2)}(\boldsymbol{r},t) - \beta_\ell p_\ell^{(1)}(\boldsymbol{r},t) = 0 \;\; \ell = 1, ..., L \tag{26}$$

with auxiliary variables $p_m^{(0)}$, $p_\ell^{(1)}$ and $p_\ell^{(2)}$ replacing their material derivatives for conciseness.
Finally, to arrive at a relation for p and p_n as required by the integral equation (14), note that, by the Euler equations for inviscid fluids, we have the relation between u_n and $\partial p/\partial n$ as

$$\frac{\partial u_n}{\partial t} + \boldsymbol{U}\cdot\nabla u_n + \frac{1}{\rho_0}\frac{\partial p}{\partial n} = 0 \tag{27}$$

where ρ_0 is the mean density of the fluid. Therefore, by applying again the material derivative operator $\frac{\partial}{\partial t} + \boldsymbol{U}\cdot\nabla$ to Eqs. (24)-(26), we get finally the coupling equations for p and p_n as follows:

$$\frac{\partial^2 p}{\partial t^2} + 2\boldsymbol{U}\cdot\nabla\frac{\partial p}{\partial t} + (\boldsymbol{U}\cdot\nabla)^2 p = -\frac{h_0}{\rho_0}\frac{\partial^2 p_n}{\partial t^2} - \frac{R_0}{\rho_0}\frac{\partial p_n}{\partial t} - \sum_{m=1}^{M} A_m p_m^{(0)} - \sum_{\ell=1}^{L}\left[B_\ell p_\ell^{(1)} + C_\ell p_\ell^{(2)}\right] \tag{28}$$

$$\frac{dp_m^{(0)}}{dt} + \lambda_m p_m^{(0)} = \frac{1}{\rho_0}\frac{\partial p_n}{\partial t}, \quad m = 1, ..., M \tag{29}$$

$$\frac{dp_\ell^{(1)}}{dt} + \alpha_\ell p_\ell^{(1)} + \beta_\ell p_\ell^{(2)} = \frac{1}{\rho_0}\frac{\partial p_n}{\partial t}, \quad \frac{dp_\ell^{(2)}}{dt} + \alpha_\ell p_\ell^{(2)} - \beta_\ell p_\ell^{(1)} = 0, \quad \ell = 1, ..., L \tag{30}$$

where again auxiliary variables $p_m^{(0)}$, $p_\ell^{(1)}$ and $p_\ell^{(2)}$ replaced their negative material derivatives for conciseness. For convenience of numerical implementation, introduce an auxiliary variable $q(\boldsymbol{r},t)$ such that

$$\frac{\partial q}{\partial t} = p \tag{31}$$

Then, equations (28)-(30) can further be written as

$$\frac{\partial p}{\partial t} + 2\boldsymbol{U}\cdot\nabla p + (\boldsymbol{U}\cdot\nabla)^2 q = -\frac{h_0}{\rho_0}\frac{\partial p_n}{\partial t} - \frac{R_0}{\rho_0}p_n - \sum_{m=1}^{M} A_m p_m^{(0)} - \sum_{\ell=1}^{L}\left[B_\ell p_\ell^{(1)} + C_\ell p_\ell^{(2)}\right] \tag{32}$$

$$\frac{dp_m^{(0)}}{dt} + \lambda_m p_m^{(0)} = \frac{1}{\rho_0}p_n, \quad m = 1, ..., M \tag{33}$$

$$\frac{dp_\ell^{(1)}}{dt} + \alpha_\ell p_\ell^{(1)} + \beta_\ell p_\ell^{(2)} = \frac{1}{\rho_0} p_n, \quad \frac{dp_\ell^{(2)}}{dt} + \alpha_\ell p_\ell^{(2)} - \beta_\ell p_\ell^{(1)} = 0, \;\; \ell = 1, ..., L \tag{34}$$

where, again for conciseness and without loss of generality, auxiliary variables $p_m^{(0)}$, $p_\ell^{(1)}$ and $p_\ell^{(2)}$ replaced their temporal anti-derivatives. We note that, in the case of no flow, time domain impedance equations (32)-(34) reduces immediately to that presented in [19].

Eq. (14) coupled with Eqs. (32)-(34) forms the integral-differential equations for the scattering solutions by surfaces with impedance boundary conditions in the presence of a uniform mean flow.

III. Multipole expansion for broadband impedance function

In this section, we describe a simple technique for finding a multipole model for the acoustic impedance function. Let the acoustic impedance $Z(\omega)$ be denoted as

$$\frac{p(\omega)}{u_w(\omega)} = Z(\omega) = R(\omega) - iX(\omega), \tag{35}$$

where $p(\omega)$ and $u_w(\omega)$ are respectively the pressure and normal velocity on the surface of liner in the frequency domain. In (35) a time dependency of $e^{-i\omega t}$ is assumed, and $R(\omega)$ is the resistance, $X(\omega)$ is the reactance. Given a set of N measurements $Z_j = Z(\omega_j)$, $j = 1, 2, ..., N$, suppose the impedance as a function of ω is to be modeled as a rational function:[6,14]

$$Z_f(\omega) = \frac{a_0 + a_1\omega + \cdots + a_\nu \omega^\nu}{b_0 + b_1\omega + \cdots + b_\mu \omega^\mu}, \tag{36}$$

which, assuming $\nu \leq \mu + 1$, may be equivalently expressed as partial fractions as

$$Z_f(\omega) = -i\omega h_0 + R_0 + \sum_{m=1}^{M} \frac{A_m}{\lambda_m - i\omega} + \frac{1}{2}\sum_{\ell=1}^{L} \left[\frac{B_\ell + iC_\ell}{\alpha_\ell + i\beta_\ell - i\omega} + \frac{B_\ell - iC_\ell}{\alpha_\ell - i\beta_\ell - i\omega} \right]. \tag{37}$$

This will be referred to as the broadband multipole model. It contains $M + 2L$ poles in the complex ω-plane. In (37), all parameters h_0, R_0, λ_m, A_m, α_ℓ, β_ℓ, B_ℓ, C_ℓ assume real values. For such a model to be physical, function $Z_f(\omega)$ should satisfy the conditions for causality, realty, and passivity,[8,18] or be a *positive-real* function as defined in [1]:

1. (Causality) $Z_f(\omega)$ is analytic (no poles) in open upper half-plane $Im\{\omega\} > 0$
2. (Realty) $Z_f(\bar{\omega}) = \bar{Z}_f(\omega)$ (an overbar denotes complex conjugate)
3. (Passivity) $Re\{Z_f(\omega)\} \geq 0$ for $Im\{\omega\} \geq 0$

These conditions lead immediately to the requirements that:[1,4]

$$h_0, R_0, \lambda_m, \alpha_\ell \geq 0 \;\text{ and }\; \nu \leq \mu + 1 \tag{38}$$

Currently, a common practice for finding the coefficients and the poles of the multipole model (37) has been to use the vector-fitting method.[9] The vector-fitting method converts a nonlinear optimization problem to a series of linear least square problems. However, a drawback of the vector-fitting method is that the passivity condition is not ensured and needs to be separately checked or enforced.[10] In what follows, we describe a minimization method for finding the poles and coefficients of the multipole model in which the passivity is always satisfied.

We note that for the partial fraction terms in (37) we have:

$$\frac{A_m}{\lambda_m - i\omega} = \frac{A_m\lambda_m + iA_m\omega}{\lambda_m^2 + \omega^2} \tag{39}$$

$$\frac{1}{2}\left[\frac{B_\ell+iC_\ell}{\alpha_\ell+i\beta_\ell-i\omega}+\frac{B_\ell-iC_\ell}{\alpha_\ell-i\beta_\ell-i\omega}\right]=\frac{\left[(\alpha_\ell B_\ell+\beta_\ell C_\ell)\left(\alpha_\ell^2+\beta_\ell^2\right)+(\alpha_\ell B_\ell-\beta_\ell C_\ell)\,\omega^2\right]+i\left[\left(2\alpha_\ell\beta_\ell C_\ell+(\alpha_\ell^2-\beta_\ell^2)B_\ell\right)\omega+B_\ell\omega^3\right]}{\left(\alpha_\ell^2+(\beta_\ell-\omega)^2\right)\left(\alpha_\ell^2+(\beta_\ell+\omega)^2\right)} \tag{40}$$

Therefore, passivity of *each* partial fraction term in (37) (those in bracket in case of paired poles), hence $Z_f(\omega)$ itself, will be ensured if we require further that

$$A_m>0,\;\;\alpha_\ell B_\ell+\beta_\ell C_\ell>0,\quad \alpha_\ell B_\ell-\beta_\ell C_\ell>0 \tag{41}$$

in addition to the requirements stipulated in (38).

Based on this observation, we propose the following minimization problem for finding the parameters of the multipole model (37):

For a given choice for M and L, find $h_0, R_0, \lambda_m, A_m, (m=1,...,M), \alpha_\ell, \beta_\ell, \gamma_\ell, \delta_\ell, (\ell=1,...,L)$ such that

$$\sum_{j=1}^{N}\left|Z_f(\omega_j;h_0,R_0,\lambda_k,A_k,\alpha_\ell,\beta_\ell,B_\ell,C_\ell)-Z_j\right|^2=\text{MINIMUM} \tag{42}$$

subject to

$$\text{(i)}\;\; h_0,R_0,\lambda_m\geq 0;\quad \text{(ii)}\;\; A_m,\alpha_\ell,\gamma_\ell,\delta_\ell>0 \tag{43}$$

where γ_ℓ and δ_ℓ are related to B_ℓ and C_ℓ as

$$B_\ell=\frac{\gamma_\ell+\delta_\ell}{2\alpha_\ell},\quad C_\ell=\frac{\gamma_\ell-\delta_\ell}{2\beta_\ell} \tag{44}$$

In the current study, the minimization problem (42) is solved using a genetic algorithm implemented in Python.

IV. Discretization

We now consider the discretization of time domain boundary integral equation (14) coupled with the impedance boundary condition formulated in Eqs. (32)-(33). Let surface S be discretized into boundary elements E_j, $j=1,2,...,N_e$, where N_e denotes the total number of elements, and let the solutions for $p(\boldsymbol{r}_s,t)$ and $p_n(\boldsymbol{r}_s,t)$ be expanded as follows:

$$p(\boldsymbol{r}_s,t)=\sum_{n=0}^{N_t}\sum_{j=1}^{N_e}u_j^n\varphi_j(\boldsymbol{r}_s)\psi_n(t) \tag{45}$$

$$p_n(\boldsymbol{r}_s,t)=\sum_{n=0}^{N_t}\sum_{j=1}^{N_e}v_j^n\varphi_j(\boldsymbol{r}_s)\psi_n(t) \tag{46}$$

where N_t denotes the total number of time steps. For any element E_j on a rigid surface, we have of course $v_j^n=0$.

For the present study, the spatial and temporal basis functions appearing in (45)-(46) are as follows:

$$\varphi_j(\boldsymbol{r}_s)=\begin{cases}1, & \boldsymbol{r}_s \text{ on element } E_j \text{ that contains node } \boldsymbol{r}_j\\ 0, & \text{otherwise}\end{cases} \tag{47}$$

and

$$\psi_n(t)=\Psi\left(\frac{t-t_n}{\Delta t}\right) \tag{48}$$

where

$$\Psi(\tau)=\begin{cases} 1+\frac{11}{6}\tau+\tau^2+\frac{1}{6}\tau^3 & -1<\tau\le 0 \\ 1+\frac{1}{2}\tau-\tau^2-\frac{1}{2}\tau^3 & 0<\tau\le 1 \\ 1-\frac{1}{2}\tau-\tau^2+\frac{1}{2}\tau^3 & 1<\tau\le 2 \\ 1-\frac{11}{6}\tau+\tau^2-\frac{1}{6}\tau^3 & 2<\tau\le 3 \\ 0 & \text{other} \end{cases} \tag{49}$$

We note that with these basis functions, the value for $p(\boldsymbol{r}_s,t)$, and similarly for $p_n(\boldsymbol{r}_s,t)$, at a time $t=t_n-\eta\Delta t$, $0\le\eta<1$, is found by the following interpolation scheme:

$$p(\boldsymbol{r}_s,t)=\varphi_j(\boldsymbol{r}_s)\left[u_j^n\Psi(-\eta)+u_j^{n-1}\Psi(1-\eta)+u_j^{n-2}\Psi(2-\eta)+u_j^{n-3}\Psi(3-\eta)\right] \tag{50}$$

Substituting (45)-(46) to the integral equation (14), and evaluating the equation at each nodal point $\boldsymbol{r}_j$ and at time level t_n, the system of discretized equations can be cast into the following matrix form:

$$\boldsymbol{B}_0\boldsymbol{u}^n+\boldsymbol{C}_0\boldsymbol{v}^n=\boldsymbol{Q}^n-\boldsymbol{B}_1\boldsymbol{u}^{n-1}-\boldsymbol{C}_1\boldsymbol{v}^{n-1}-\boldsymbol{B}_2\boldsymbol{u}^{n-2}-\boldsymbol{C}_2\boldsymbol{v}^{n-2}-\cdots-\boldsymbol{B}_J\boldsymbol{u}^{n-J}-\boldsymbol{C}_J\boldsymbol{v}^{n-J} \tag{51}$$

where $\boldsymbol{u}^k$ and $\boldsymbol{v}^k$ denote respectively all unknowns $\left\{u_j^k, j=1,2,...,N_e\right\}$ and $\left\{v_j^k, j=1,2,...,N_e\right\}$, at time level t_k, and $\boldsymbol{Q}^n$stands for the contribution from the source term (9). In Eq. (51), J represents the maximum time history required for the solution of the boundary integral equation.

The non-zero entries of matrices $\boldsymbol{B}_k$ and $\boldsymbol{C}_k$, $k=1,2,...,J$, in (51) are:

$$\{\boldsymbol{B}_k\}_{ij}=2\pi a\delta_{ij}\psi'_{n-k}(t_n)+a\int_{E_j}\frac{\partial G_0}{\partial\bar{n}}\left(\psi'_{n-k}(t_R^n)+\frac{\bar{R}}{c\alpha^2}\psi''_{n-k}(t_R^n)\right)d\boldsymbol{r}_s+bc\delta_{ij}\delta_{k0}D_i$$

$$+bc\int_{E_j}\frac{\partial^2 G_0}{\partial\bar{n}'\partial\bar{n}}\left(\psi_{n-k}(t_R^n)-\delta_{ij}\psi_{n-k}(t_n)+\frac{\bar{R}}{c\alpha^2}\psi'_{n-k}(t_R^n)\right)d\boldsymbol{r}_s+\frac{b}{c\alpha^4}\int_{E_j}\bar{R}^3\frac{\partial G_0}{\partial\bar{n}'}\frac{\partial G_0}{\partial\bar{n}}\psi''_{n-k}(t_R^n)d\boldsymbol{r}_s \tag{52}$$

$$\{\boldsymbol{C}_k\}_{ij}=-a\int_{E_j}G_0\psi'_{n-k}(t'_R)d\boldsymbol{r}_s+2\pi bc\delta_{ij}\psi_{n-k}(t_n)-bc\int_{E_j}\frac{\partial G_0}{\partial\bar{n}'}\left(\psi'_{n-k}(t_R^n)+\frac{\bar{R}}{c\alpha^2}\psi''_{n-k}(t_R^n)\right)d\boldsymbol{r}_s \tag{53}$$

Here, primes over the temporal basis functions indicate derivative. In (52)-(53), δ_{ij} and δ_{k0} are Kronecker delta functions and D_i in (52) denotes the following integral:[11]

$$D_i=-\int_{S-E_i}\frac{\partial^2 G_0}{\partial\bar{n}'\partial\bar{n}}(\boldsymbol{r}_s,\boldsymbol{r}_i)d\boldsymbol{r}_s$$

To discretize the liner differential equations (32)-(34), we expand the auxiliary variables on *every collocation point on the liner surface* as:

$$p_m^{(0)}(t)=\sum_{n=0}^{N_t}w_{0,m}^n\psi_n(t),\quad m=1,2,...,M \tag{54}$$

$$p_\ell^{(1)}(t)=\sum_{n=0}^{N_t}w_{1,\ell}^n\psi_n(t),\quad p_\ell^{(2)}(t)=\sum_{n=0}^{N_t}w_{2,\ell}^n\psi_n(t),\quad \ell=1,2,...,L \tag{55}$$

$$q(t)=\sum_{n=0}^{N_t}q^n\psi_n(t) \tag{56}$$

where $w^n_{0,m}$,$w^n_{1,\ell}$, $w^n_{2,\ell}$, and q^n are the expansion coefficients and the time basis function $\psi_n(t)$ is as given in (48). In particular, we note that $\psi_n(t_k) = \delta_{nk}$ for the temporal basis function given in (48).

Eqs. (32)-(34) are now discretized as follows:

$$\frac{1}{\Delta t}\sum_{k=0}^{3} u_j^{n-k}\Psi'(k) + 2\left[\boldsymbol{U}\cdot\nabla p\right]_j^n + \left[(\boldsymbol{U}\cdot\nabla)^2 q\right]_j^n + \frac{h_0}{\rho_0\Delta t}\sum_{k=0}^{3} v_j^{n-k}\Psi'(k) + \frac{R_0}{\rho_0}v_j^n + \sum_{m=1}^{M} A_m w^n_{0,m} + \sum_{\ell=1}^{L}\left[B_\ell w^n_{1,\ell} + C_\ell w^n_{2,\ell}\right] = 0 \tag{57}$$

$$\frac{1}{\Delta t}\sum_{k=0}^{3} w_{0,m}^{n-k}\Psi'(k) + \lambda_m w^n_{0,m} = \frac{1}{\rho_0}v_j^n, \quad m = 1, ..., M \tag{58}$$

$$\frac{1}{\Delta t}\sum_{j=0}^{3} w_{1,\ell}^{n-j}\Psi'(j) + \alpha_\ell w^n_{1,\ell} + \beta_\ell w^n_{2,\ell} = \frac{1}{\rho_0}v_j^n, \quad \frac{1}{\Delta t}\sum_{j=0}^{3} w_{2,\ell}^{n-j}\Psi'(j) + \alpha_\ell w^n_{2,\ell} - \beta_\ell p^n_{1,\ell} = 0, \quad \ell = 1, ..., L \tag{59}$$

This is akin to discretizing Eqs. (32)-(34) by the third-order backward difference scheme.[2,19]

In the above, $\left[\boldsymbol{U}\cdot\nabla p\right]_j^n$ and $\left[(\boldsymbol{U}\cdot\nabla)^2 q\right]_j^n$ denote respectively the discretized pressure stream-wise derivative term and the term for the second stream-wise derivative of q, hereby referred to as the q-term, for element E_j at time t_n.

Introduce a vector $\bar{\boldsymbol{s}}$ of dimension $M + 2L$ that contains all auxiliary variables at a liner point as

$$\bar{\boldsymbol{s}}^n \equiv \left[\begin{array}{cccccccccccc} w^n_{0,1} & w^n_{0,2} & ... & w^n_{0,M} & w^n_{1,1} & w^n_{2,1} & w^n_{1,2} & w^n_{2,2} & ... & w^n_{1,L} & w^n_{2,L} \end{array}\right]^T$$

Then, Eq. (57) can be written succinctly as the following iteration scheme for a node on element E_j and time t_n:

$$d_0 u_j^n + e_0 v_j^n + d_1 u_j^{n-1} + e_1 v_j^{n-1} + d_2 u_j^{n-2} + e_2 v_j^{n-2} + d_3 u_j^{n-3} + e_3 v_j^{n-3} + \boldsymbol{f}_0^T\bar{\boldsymbol{s}}^n + \left[2\boldsymbol{U}\cdot\nabla p\right]_j^n + \left[(\boldsymbol{U}\cdot\nabla)^2 q\right]_j^n = 0 \tag{60}$$

and Eqs. (58)-(59) can be written as

$$\bar{\boldsymbol{H}}_0\bar{\boldsymbol{s}}^n + d_1\bar{\boldsymbol{s}}^{n-1} + d_2\bar{\boldsymbol{s}}^{n-2} + d_3\bar{\boldsymbol{s}}^{n-3} + v_j^n\boldsymbol{g}_0 = 0 \tag{61}$$

where the coefficients are the following:

$$d_0 = \frac{1}{\Delta t}\Psi'(0), \quad e_0 = \frac{1}{\rho_0}h_0 d_0 + \frac{1}{\rho_0}R_0; \quad d_k = \frac{1}{\Delta t}\Psi'(k), \quad e_k = \frac{1}{\rho_0}h_0 d_k, \quad k = 1, 2, 3$$

$$[\boldsymbol{f}_0, \boldsymbol{g}_0] = \left[\begin{array}{cccccccccccc} A_1 & A_2 & ... & A_M & B_1 & C_1 & B_2 & C_2 & ... & B_L & C_L \\ -\frac{1}{\rho_0} & -\frac{1}{\rho_0} & ... & -\frac{1}{\rho_0} & -\frac{1}{\rho_0} & 0 & -\frac{1}{\rho_0} & 0 & ... & -\frac{1}{\rho_0} & 0 \end{array}\right]^T$$

$$\bar{\boldsymbol{H}}_0 = d_0\boldsymbol{I} + \left[\begin{array}{cccccccc} \gamma_1 & & & & & & & \\ & ... & & & & & & \\ & & \gamma_M & & & & & \\ & & & \alpha_1 & \beta_1 & & & \\ & & & -\beta_1 & \alpha_1 & & & \\ & & & & & ... & & \\ & & & & & & \alpha_L & \beta_L \\ & & & & & & -\beta_L & \alpha_L \end{array}\right]_{(M+2L)\times(M+2L)}$$

where $\boldsymbol{I}$ is the identity matrix and a superscript T indicates matrix transpose.

When Eqs. (60)-(61) are applied to all liner points, we get the following algebraic system as a result of the liner impedance boundary condition:

$$\boldsymbol{D}_0\boldsymbol{u}^n + \boldsymbol{E}_0\boldsymbol{v}^n + \boldsymbol{F}_0\boldsymbol{s}^n + 2\mathcal{X}_1\boldsymbol{u}^n + \mathcal{X}_2\boldsymbol{q}^n = -\boldsymbol{D}_1\boldsymbol{u}^{n-1} - \boldsymbol{E}_1\boldsymbol{v}^{n-1} - \boldsymbol{D}_2\boldsymbol{u}^{n-2} - \boldsymbol{E}_2\boldsymbol{v}^{n-2} - \boldsymbol{D}_3\boldsymbol{u}^{n-3} - \boldsymbol{E}_3\boldsymbol{v}^{n-3} \quad (62)$$

$$\boldsymbol{G}_0\boldsymbol{v}^n + \boldsymbol{H}_0\boldsymbol{s}^n = -\boldsymbol{D}_1\boldsymbol{s}^{n-1} - \boldsymbol{D}_2\boldsymbol{s}^{n-2} - \boldsymbol{D}_3\boldsymbol{s}^{n-3} \quad (63)$$

where vectors $\boldsymbol{u}^n$, $\boldsymbol{v}^n$ and $\boldsymbol{s}^n$denote the variables of all collocation points on the liner surface at time level t_n, namely, respectively for $\{u_i^n, i = 1, 2, ..., N_l\}$, $\{v_i^n, i = 1, 2, ..., N_l\}$ and $\{\boldsymbol{s}_i^n, i = 1, 2, ..., N_l\}$ in which N_l is the total number of liner nodal points. The matrices in (62)-(63) are the following:

$$\boldsymbol{F}_0 = \boldsymbol{I} \otimes \boldsymbol{f}_0^T, \quad \boldsymbol{G}_0 = \boldsymbol{I} \otimes \boldsymbol{g}_0^T, \quad \boldsymbol{H}_0 = \boldsymbol{I} \otimes \bar{\boldsymbol{H}}_0; \quad \boldsymbol{D}_j = \boldsymbol{I} \otimes d_j, \quad \boldsymbol{E}_j = \boldsymbol{I} \otimes e_j, \quad j = 0, 1, 2, 3$$

where $\boldsymbol{I}$ stands for the identity matrix and $\otimes$ is the matrix Kronecker product notation. Also, matrices $\mathcal{X}_1$ and $\mathcal{X}_2$ in Eq. (62) denote the discretization matrix operators for the pressure derivative term $[\boldsymbol{U} \cdot \nabla p]_j^n$ and the q-term $\left[(\boldsymbol{U} \cdot \nabla)^2 q\right]_j^n$ respectively. For the current work, second-order central difference schemes are used for spatial derivative approximations.

Eqs. (51) and (62)-(63) form the discretization scheme for the time domain boundary integral equation and time domain impedance condition.

V. Numerical example

Formulation and implementation of a time domain broadband impedance boundary condition as outlined in previous sections will be validated using the GFIT experimental database.[13] To this end, the inherently internal duct propagation problem is cast as an external scattering problem in an open-ended duct configuration. A duct geometry is constructed where its interior surfaces reproduce the ducted environment in the GFIT experiments while external and terminating surfaces are added such that a closed scattering body surface is formed, as shown in Figure 2. In addition, the source function $s(\boldsymbol{r}, t)$ in (9) is so formulated such that an incident plane wave is generated in the ducted region. The time domain impedance boundary condition is applied on a section of the duct interior surface where the acoustic liner is installed. In this way, propagation and scattering of the plane wave mode by the liner section are computed as a time domain scattering problem. The acoustic field by computation will be compared to that by the experiment.

Figure 2. Modeling of an internal ducted environment as an external scattering problem. Liner section inside the duct is noted by the darkened area.

V.A. Formulation of incident plane wave

To impose an incident plane wave (zero-th order mode) inside the duct as in the GFIT experiments, the source term for the wave equation (1) is chosen to be

$$s(\boldsymbol{r},t) = \Phi_0'(t)\delta(x-x_0), \quad (y,z) \in [0,L_y] \times [-L_z/2, L_z/2] \tag{64}$$

where $\Phi_0(t)$ is some chosen function of t and a prime denotes the time derivative, x_0 is the x-coordinate for the location (referred to as the source plane, where the plane wave is to be introduced), and L_y and L_z denote the dimensions of the duct cross section in y and z directions, respectively. For the results reported in this section, the boundary element model for the duct extends from $x = -2.5$ to $x = 2.0$. Throughout this section, the length unit is meters (m). The duct cross section is such that $L_y = 0.0635$ and $L_z = 0.0508$ as in the GFIT experiments. A liner section is installed at the upper surface of the duct from $x = 0.2125$ to $x = 0.8125$ and $y = L_y$. The source location is $x_0 = -0.1$, sufficiently away from the leading edge of the liner section. Solving wave equation (1) with a source term as given in (64), it can be shown that the acoustic pressure $p(\boldsymbol{r},t)$ generated by (64) inside a duct of solid surfaces is of plane waves of the form

$$p(\boldsymbol{r},t) = \Phi_0\left(t + \beta(x-x_0) - |x-x_0|/\alpha^2 c\right) = \begin{cases} \Phi_0\left(t - \frac{x-x_0}{U_1+c}\right) & x > x_0 \\ \Phi_0\left(t - \frac{x-x_0}{U_1-c}\right) & x < x_0 \end{cases}, \quad (y,z) \in [0,L_y] \times [-L_z/2, L_z/2] \tag{65}$$

Eq. (65) represents two *independent* plane waves (zero-th order mode) propagating at a speed of $U_1 + c$ and $U_1 - c$ to the right and left, respectively, of the source plane location $x = x_0$. Here, U_1 denotes the stream-wise uniform mean flow velocity inside the duct.

For the current computation, the source time function in (64) is taken to be the following broadband Gaussian function:

$$\Phi_0(t) = e^{-\sigma t^2} \tag{66}$$

where $\sigma = 1.42/(3\Delta t)^2$. With the given source term (64), the source integral (9) reduced to a double integral over the source plane at $x = x_0$ which is evaluated using high-order quadrature. While the plane waves will eventually be reflected at both ends of the duct, the time domain solution is to be stopped before the reflected waves reach the measurement zone which is located at the side of the duct opposite to the liner section from $x = 0$ to $x = 1$.

V.B. Numerical results and comparison with experimental data

In the GFIT experiments used in the current comparison,[13] the mean flow is non-uniform with a center-line Mach number of 0.3. For the results reported here, a uniform mean flow of Mach number 0.2 is assumed for computation as a constant mean flow is required for the boundary integral equation formulation. The liner in the study consists of a 1.5-inch deep core covered with a wire mesh face-sheet with DC flow resistance $R_f = 1.3\rho_0 c$. Microphones are mounted on the lower wall ($y = 0$) opposite the liner section from $x = 0$ to $x = 1$ to measure the pressure field. Based on the experimental measurements, the impedance of the liner is educed at a set of discrete frequencies from 400Hz to 3000Hz. The resistance and reactance of the liner used here are plotted in symbols in Fig. 3.

Using the experimentally educed impedance data, a liner impedance function is approximated by the broadband multipole impedance model Eq. (20) with fitted parameters using one single pole and three paired poles (i.e., $M = 1$, $L = 3$). The minimization problem formulated in (42)-(44) is solved using a genetic algorithm implemented in Python. The resistance and reactance predicted by the multipole model are also plotted in Fig. 3. The parameters for the multipole model are (non-dimensionalized by $\rho_0 c$ for impedance, $c/\mathcal{L}$ for frequency where length scale $\mathcal{L} = 1(m)$):

$$R_0 = 0.1,\ h_0 = 0.04,\ \lambda = 4.75,\ A_1 = 36.55,\ \alpha_1 = 7.46,\ \beta_1 = 36.98,\ B_1 = 6.74,\ C_1 = 1.33$$

$$\alpha_2 = 6.6,\ \beta_2 = 44.96,\ B_2 = 7.25,\ C_2 = 0.85,\ \alpha_3 = 7.67,\ \beta_3 = 24.51,\ B_3 = 11.32,\ C_3 = 0.52$$

Fig. 4 shows an example of computed pressure time history at coordinates $\boldsymbol{r} = (0.5, 0, 0)$ on the duct surface opposite to the liner section. The solution without the liner impedance condition are plotted as the dotted line. It is simply a Gaussian-shaped pulse as predicted by (65). The numerical solution computed with the liner impedance condition but without the q-term is shown in solid line and that with the q-term is shown in dashed line. Due to the effects of liner, the magnitude of the incident pressure pulse is significantly reduced as expected. However, the solution computed with the q-term eventually becomes exponentially large due to the Kelvin-Helmholtz instability that is intrinsic to the vortex sheet included in the Ingard-Myers impedance condition for a liner with flow. On the other hand, the numerical solution computed without the q-term remained stable. More importantly, both solutions matched very well until the on-set of the exponentially growing solution. This suggests that neglecting the q-term in the impedance boundary condition formulation (32) would not substantially alter numerical simulation results for the interaction of acoustic waves and the liner, at least for the current Mach number of 0.2, but could effectively suppress the Kelvin-Helmholtz instability that is intrinsic in the Ingard-Myers condition.

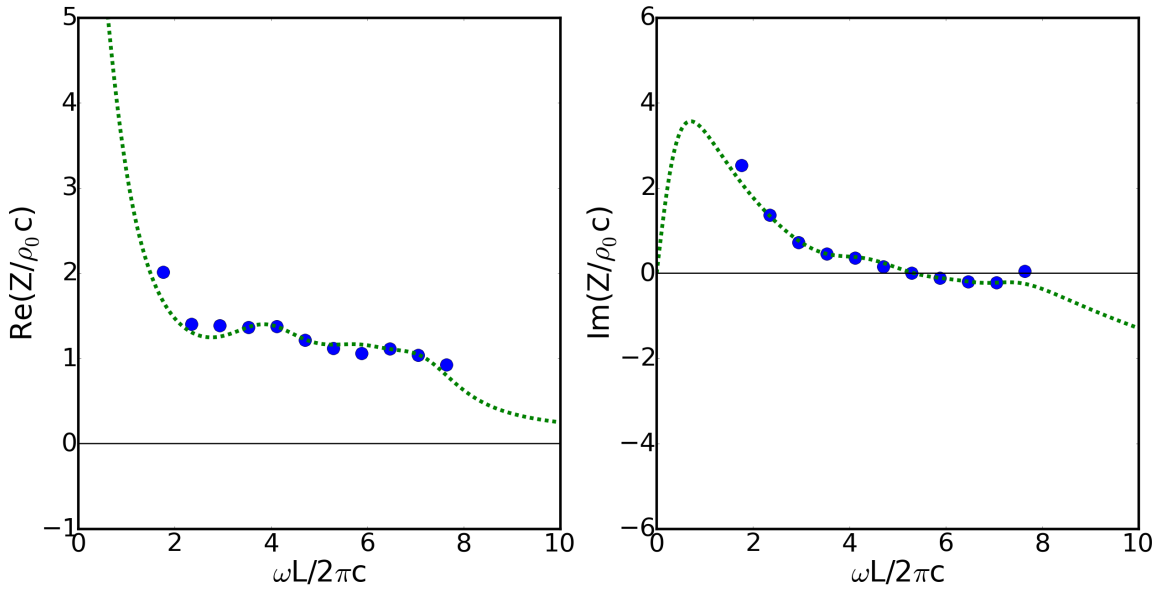

Figure 3. An example of broadband multipole impedance model (20) fitted for a liner of perforated plate with cavity of depth 1.5 in and wired mesh face sheet of resistance $R = 1.3\rho_0 c$. Symbols denote the measured impedance value and dashed lines denote the broadband impedance model. Here frequency is non-dimensionalized by c/L where L=1(m) and c=343 (m/s).

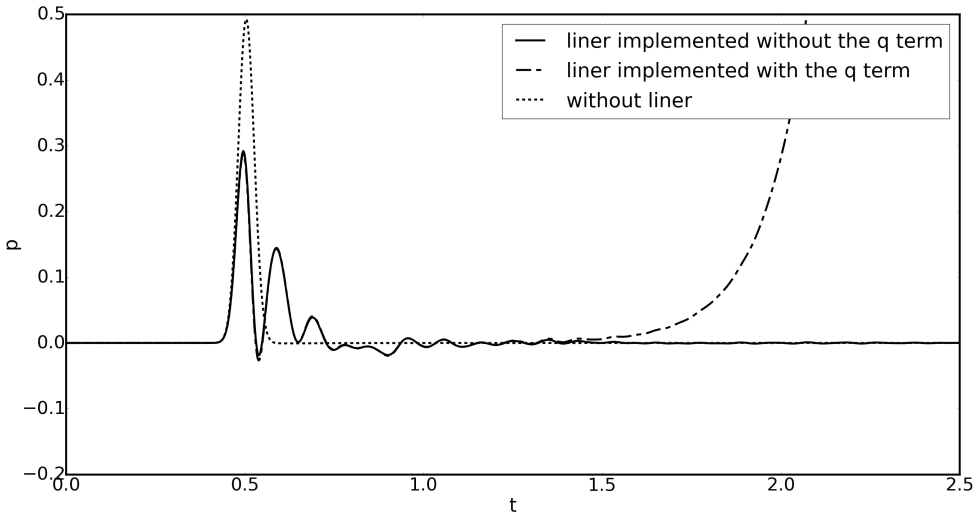

Figure 4. pressure time history at a point on the duct surface opposite to the liner section at coordinates $\boldsymbol{r} = (0.5, 0, 0)$. The solution without the liner impedance condition are plotted in the dotted line. The numerical solution computed with the liner impedance condition but without the q-term is shown in solid line and that with the q-term is shown in dashed line.

Figure 5 shows stacked snapshots of pressure variation along the duct interior surface opposite to the liner section. As one of the plane wave pulses propagates to the right of the source location, the effects of liner on the incident pressure pulse are clearly seen and captured by computation. Also visible are the reflections of the incident plane wave by the leading edge of the liner section.

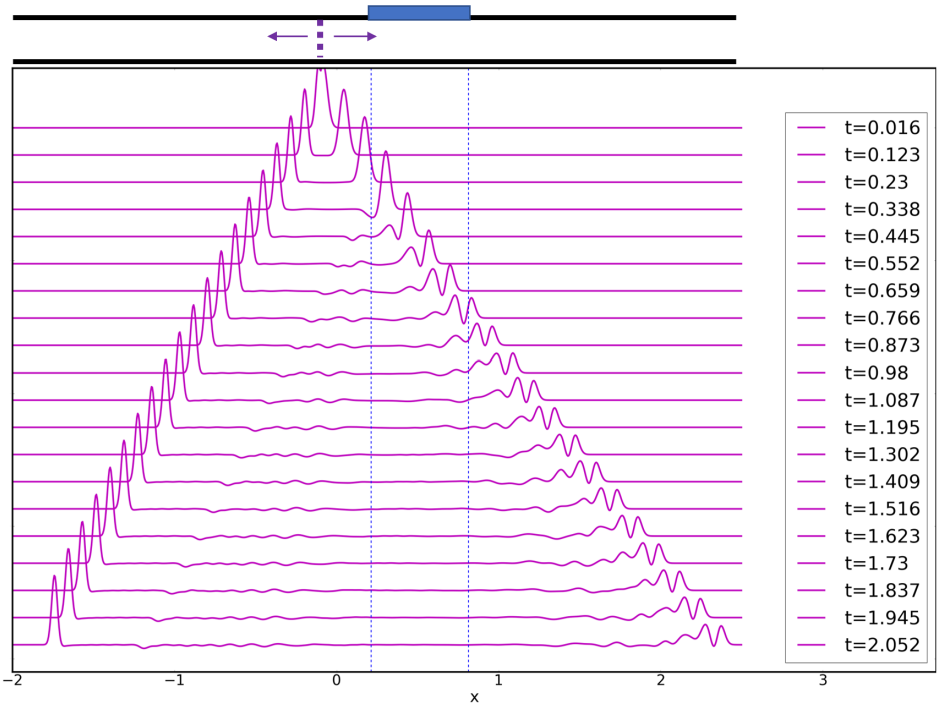

Figure 5. Stacked snapshots of pressure along the ducted side-wall opposite to the side of the liner at selected times as indicated. A broadband plane wave is introduced near the liner section as indicated.

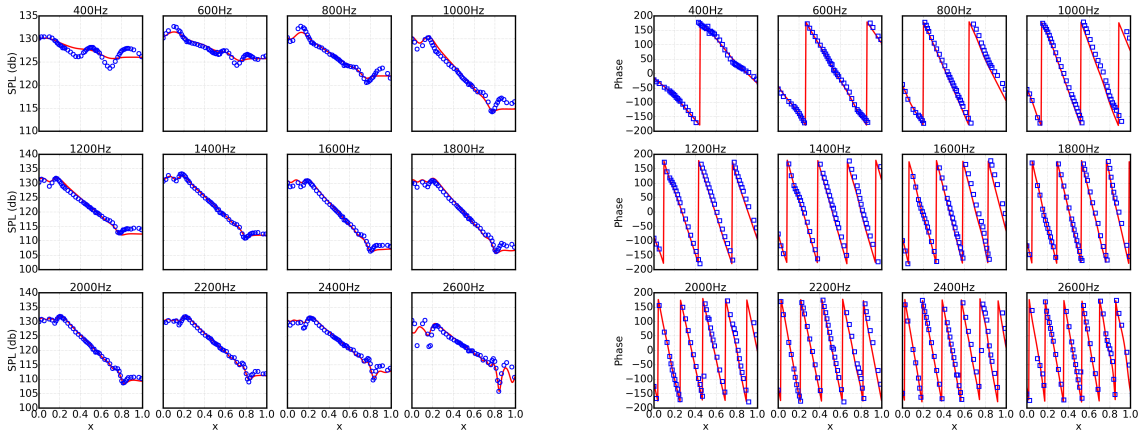

Figure 6. Left: SPL v.s. x at selected frequencies as indicated; Right: Phase v.s. x. Flow Mach number is $M = 0.2$. Perforated plate liner has cavity depth of 1.5 in and face-sheet DC flow resistance $R_f \approx 1.3\rho_0 c$. Line: computation; Symbol: experiment.

With time domain solution, the frequency domain results can be obtained readily by FFT (Fast Fourier Transform) or the following summation:

$$\hat{p}(\boldsymbol{r},\omega) = \Delta t \left[p(\boldsymbol{r},t_1)e^{i\omega t_1} + p(\boldsymbol{r},t_2)e^{i\omega t_2} + p(\boldsymbol{r},t_3)e^{i\omega t_3} + \cdots\cdots + p(\boldsymbol{r},t_{N_t})e^{i\omega t_{N_t}} \right] \tag{67}$$

Figure 6 shows a comparison of computed and experimental results for the pressure distribution along the wall opposite to the liner section at selected frequencies. For the results shown, the time domain solution is computed without the q-term. Very good agreement is seen for all the frequencies, demonstrating the validity of the current formulation.

VI. Conclusions

A time domain boundary integral equation, with Burton-Miller type reformulation, has been presented for acoustic scattering by lined surfaces in a uniform mean flow. The Ingard-Myers liner impedance boundary condition has been implemented using a time domain broadband multipole model for the impedance which results in additional differential equations that augment the boundary integral equation. While the Ingard-Myers condition is known to support Kelvin-Helmholtz instability due to its use of a vortex sheet interface between the flow and the liner surface, it is found that by neglecting a second derivative term in the current time domain impedance boundary condition formulation, the instability can be effectively suppressed in computation without substantially impact the solution for the acoustic pressure. In fact, it can be shown that neglecting the q-term in the time domain impedance condition formulation (32)-(34) is equivalent to equating u_n and u_w in the liner model, thereby romving the vortex sheet, and using a mean flow that is twice of its actual value. This may provide potentially a simple and practical way for circumventing the intrinsic instability in the Ingard-Myers impedance boundary condition formulation with flow of low Mach numbers. Discretization of the coupled integral-differential equations by a time domain boundary element method has been described. The current formulation and implementation are validated using a NASA Langley GFIT experimental dataset.

Moreover, a minimization procedure has been proposed for finding the poles and coefficients of the multipole impedance model. Unlike the vector-fitting method, passivity of the model is ensured. Numerical test cases have shown that the proposed approach is effective for fitting the resistance and reactance of liners that are commonly used in aeroacoustics applications.

Acknowledgments

This research was funded by the Advanced Air Transport Technology (AATT) Project of the NASA Advanced Air Vehicles Program (AAVP). This work used the computational resources at the Old Dominion University ITS Turing cluster.

References

[1]O. Brune, "Synthesis of a finite two-terminal network whose driving-point impedance is a prescribed function of frequency, J. Math. Phy., Vol. 10, 191-236, (1931)

[2]Butcher, J., *Numerical Methods for Ordinary Differential Equations*, 3rd ed., Wiley, New York, 2016.

[3]A. J. Burton and G. F. Miller, The application of integral equation methods to the numerical solution of some exterior boundary-value problems, Proc.R.Soc.London, Ser A, Vol. 323, 201-210, 1971.

[4]W.-K. Chen, Passive, Active, and Digital Filters, CRC Press, (2009)

[5]D. J. Chappell, P. J. Harris, D. Henwood, and R. Chakrabarti, A stable boundary element method for modeling transient acoustic radiation, Journal of the Acoustical Society of America, Vol. 120, 74–80, 2006.

[6]D. Dragna, P. Pineau, and P. Blanc-Benon, "A Generalized Recursive Convolution Method for Time-Domain Propagation in Porous Media," Journal of the Acoustical Society of America, Vol. 138, 1030–1042, (2015)

[7]A. A. Ergin, B. Shanker, and E. Michielssen, Analysis of transient wave scattering from rigid bodies using a Burton–Miller approach, Journal of the Acoustical Society of America, Vol. 106, 2396–2404 (1999).

[8]K.-Y. Fung and H. Ju, "Time-domain impedance boundary conditions for computational acoustics and aeroacoustics", International Journal of Computational Fluid Dynamics, Vol. 18, 503-511, (2004)

[9]B. Gustavsen and A. Semlyen, Rational approximation of frequency domain responses by vector fitting, IEEE Transactions on Power Delivery, Vol. 14, 1052 - 1061, 1999.

[10]B. Gustavsen and A. Semlyen, Enforcing passivity for admittance matrices approximated by rational functions, IEEE Transactions on Power Systems, Vol. 16, 97–104, 2001.

[11]F. Q. Hu, M. E. Pizzo, and D. M. Nark, On a time domain boundary integral equation formulation for acoustic scattering by rigid bodies in uniform mean flow , Journal of the Acoustical Society of America, Vol. 142, 3624-3636, 2017.

[12]U. Ingard, "Influence of fluid motion past a plane boundary on sound reflection, absorption, and transmission," J. Acoust. Soc. Am., Vol. 31, 1035,1959.

[13]M. Jones and W. Watson, "On the Use of Experimental Methods to Improve Confidence in Educed Impedance", AIAA paper 2011-2865, 2011.

[14]X. Y. Li, X. D. Li, and C. K. W. Tam, "Improved Multipole Broadband and Time-Domain Impedance Boundary Condition," AIAA Journal, Vol. 50, 980–984, (2012)

[15]C.Chen and X. D. Li, Numerical Efficiency Analysis of Multi-pole Time-domain Impedance Boundary Conditions, 8th European Conference for Aeronautics and Aerospace Sciences, Madrid, Spain, July 1-4, 2019, https://doi.org/10.13009/EUCASS2019-1034.

[16]M. Myers, "On the acoustic boundary condition in the presence of flow," J. Sound Vib. Vol. 71, 429–434, 1980.

[17]Y. Reymen, M. Baelmans, and W. Desmet, Efficient implementation of Aam and Auriault's time-domain impedance boundary condition, AIAA Journal, Vil. 46, 2368–2376, 2008.

[18]S. W. Rienstra, "Impedance Models in Time-Domain Including the Extended Helmholtz Resonator Model," American Institute of Aeronautics and Astronautics, AIAA paper 2006–2686, (2006)

[19]M. E. Rodio, F. Q. Hu, and D. M. Nark, Time-Domain Boundary Element Method with Broadband Impedance Boundary Condition, AIAA Journal, Feb., 2022, https://doi.org/10.2514/1.J060614.

[20]C. K. W. Tam and L. Auriault, Time-domain impedance boundary conditions for computational aeroacoustics, AIAA Journal, Vol. 34, 917–923, 1996.